

# 1 Seasonal dynamics of closed shallow lakes nutrient status controlled 2 by lacustrine groundwater discharge

3 Xiaoliang Sun<sup>1,2</sup>, Yao Du<sup>1,2\*</sup>, Hao Tian<sup>1,2</sup>, Jiawen Xu<sup>1,2</sup>, Huanhuan Shi<sup>1,2</sup>, Yetong Liu<sup>1,2</sup>, Yamin Deng<sup>1,2</sup>,  
4 Yiqun Gan<sup>1,2</sup>, Yanxin Wang<sup>1,2</sup>

5 <sup>1</sup>Key Laboratory of Groundwater Quality and Health (China University of Geosciences), Ministry of  
6 Education, Wuhan 430078, China.

7 <sup>2</sup>School of Environmental Studies & State Key Laboratory of Geomicrobiology and Environmental  
8 Changes, China University of Geosciences, Wuhan 430078, China.

9 Corresponding: Yao Du (yaodu@cug.edu.cn)

10  
11 **Abstract.** Lacustrine groundwater discharge (LGD) and its associated nitrogen (N) and phosphorus (P)  
12 inputs are increasingly recognized as the critical drivers of lake eutrophication. However, the  
13 intermonthly variability in LGD and its influence on lake nutrient dynamics remain poorly understood.  
14 In this study, high-frequency monitoring and hydrochemical analyses were conducted over a full  
15 hydrological year to investigate LGD-related nutrient fluxes and their effects in a typical oxbow lake in  
16 the central Yangtze Basin. Water level data and <sup>222</sup>Rn tracing revealed a seasonal LGD pattern  
17 characterized by an increase from summer to winter, followed by a decline from winter to spring, with  
18 LGD rates ranging from 35.36 to 51.71 mm·d<sup>-1</sup>. This pattern was regulated by monthly net  
19 precipitation, which controlled the lake level fluctuations and LGD rates. The corresponding N and P  
20 loads varied synchronously with LGD and showed seasonal synchrony with lake N and P  
21 concentrations. Moreover, variations in the N/P ratio carried by LGD regulate the lake water N/P ratio,  
22 thereby influencing its relationship with the dynamic changes in chlorophyll-a. A large number of  
23 typical closed shallow lakes similar to the studied cases exist worldwide, and therefore, the regulatory  
24 role of LGD on lake nutrient status revealed in this study can be reasonably extended to other closed  
25 shallow lake systems. This study provides the first evidence that groundwater-driven nutrient loading  
26 influences lake nutrient status on an intermonthly scale, offering new insights and management  
27 strategies for eutrophication control in closed shallow lake systems worldwide.

## 28 29 1 Introduction

30 Lakes are vital terrestrial ecosystems with ecological, environmental, and societal importance  
31 (Zedler and Kercher, 2005). A number of studies have highlighted that lacustrine groundwater  
32 discharge (LGD) not only sustains the lake water balance but also serves as a key pathway for nitrogen  
33 (N) and phosphorus (P) inputs, significantly influencing biogeochemical cycling (Meinikmann et al.,  
34 2015; Rosenberry et al., 2015; Luo et al., 2018; Kazmierczak et al., 2020; Lewandowski et al., 2024).  
35 By altering nutrient concentrations, LGD can regulate lake trophic status and contribute to  
36 eutrophication (Shi et al., 2022; Zheng et al., 2025). Thus, understanding LGD’s impact on lake water  
37 environments is critical for elucidating eutrophication mechanisms.

38 The LGD rate exhibits pronounced temporal variability over the hydrological year, primarily  
39 influenced by the combined effects of hydrological and meteorological factors (Burnett et al., 2017; Shi  
40 et al., 2022; Sun et al., 2024). **In relatively closed lake systems (lacking perennial surface river inflows  
41 or where inflowing runoff has minimal impact on hydrodynamics, water balance, or residence time),  
42 meteorological factors are generally the dominant drivers of LGD.** However, the magnitude and  
43 direction of these influences vary considerably across regions. **For example, studies in Lake Taihu  
44 indicate that evaporation can enhance LGD by regulating lake water levels (Shi et al., 2022) (four  
45 sampling campaigns); research in Huixian Lake in karst regions shows that precipitation can promote  
46 LGD by elevating groundwater levels (two sampling campaigns) (Zhang et al., 2024); whereas studies  
47 of subsidence lakes in coal mining areas have found that both precipitation and evaporation are  
48 negatively correlated with LGD, suggesting a complex influence mechanism of meteorological factors  
49 (four sampling campaigns) (Jiang et al., 2024).** Although these studies have provided valuable insights,  
50 most observations are limited to extreme hydrological periods (e.g., wet and dry seasons) or are  
51 conducted at seasonal resolution (four sampling campaigns), generally lacking continuous monitoring  
52 with high-frequency. As a result, understanding of LGD dynamics at the monthly scale remains limited.  
53 **However, the responses of lake water levels and groundwater levels to precipitation and evaporation  
54 typically occur on a monthly timescale, making it difficult for low-frequency or seasonal observations  
55 to effectively capture how water level fluctuations regulate LGD.** In particular, along the process  
56 pathway of “precipitation/evaporation → lake/groundwater levels → LGD,” the mechanistic linkages  
57 remain insufficiently understood. **Therefore, compared to the low-frequency monitoring commonly  
58 adopted in existing studies, high-frequency observations at the monthly scale can provide new insights  
59 and evidence for elucidating intra-seasonal LGD processes—an important scientific issue that has not**

60 yet received adequate attention in previous research.

61 In existing studies, groundwater is regarded not only as an important source of lake water recharge,  
62 but also as a major contributor of nitrogen and phosphorus inputs to lakes. In some lakes, LGD  
63 contributes more than 50%, and in certain cases, over 90% of the total nitrogen (N) and phosphorus (P)  
64 inputs often exceed those from surface inflows (Stets et al., 2010; Meinikmann et al., 2015; Shi et al.,  
65 2022). Once discharged, groundwater-derived nutrients undergo biogeochemical transformations or are  
66 assimilated by aquatic organisms, thereby affecting the primary productivity and eutrophication (Zheng  
67 et al., 2025). For instance, LGD-driven nutrient inputs have been shown to stimulate chlorophyll *a* (Chl  
68 *a*) production in closed lakes and alter nutrient limitation patterns via shifts in N/P ratios (Xu et al.,  
69 2025). In Taihu Lake, LGD-derived N inputs were found to alleviate N limitation (Zheng et al., 2025).  
70 However, most studies have focused on nutrient flux quantification over discrete periods, with limited  
71 insight into the temporal variability and trophic responses of lakes. Understanding the monthly-scale  
72 variations and their controlling mechanisms is essential not only for predicting responses to extreme  
73 hydrological events but also for identifying critical periods of nutrient input that drive eutrophication.

74 Environmental tracers are increasingly applied in studies of LGD. An ideal tracer typically  
75 exhibits significant concentration differences between lake water and groundwater (often spanning  
76 orders of magnitude) and stable chemical properties (Arnoux et al., 2017; Petermann et al., 2018).  
77 Commonly used tracers include  $^{222}\text{Rn}$ ,  $^{226}\text{Ra}$ , stable hydrogen and oxygen isotopes ( $\delta^2\text{H}$ ,  $\delta^{18}\text{O}$ ),  $\text{Cl}^-$ , and  
78 electrical conductivity. Among these,  $^{222}\text{Rn}$  and  $^{226}\text{Ra}$  often show concentration differences of up to  
79 two-three orders of magnitude between the two water types, whereas differences in  $\text{Cl}^-$  and electrical  
80 conductivity are generally smaller (sometimes only several times). Therefore,  $^{222}\text{Rn}$  and  $^{226}\text{Ra}$  are  
81 frequently the preferred tracers in LGD studies, with other indicators used as auxiliaries when  
82 conditions permit (Dimova & Burnett., 2011). The applicability of stable hydrogen and oxygen  
83 isotopes is strongly influenced by hydrological stability; in lakes with pronounced seasonal  
84 hydrological fluctuations, their quantitative accuracy may be significantly reduced (Sun et al., 2025a).  
85 Regarding radioactive tracers,  $^{226}\text{Ra}$  primarily desorbs from particles into the water phase in brackish or  
86 saline environments (Webster et al., 1995; Gonnee et al., 2008), and its concentration is typically low  
87 in freshwater lakes. Consequently, in freshwater lake LGD studies,  $^{222}\text{Rn}$  is more commonly used and  
88 effective due to its high solubility, large concentration gradient, and ease of detection.

89 The middle Yangtze River plain is characterized by a high density of lakes, and previous studies

90 have shown that lakes of different types commonly exhibit groundwater discharge of varying  
91 intensities, along with associated nitrogen and phosphorus input fluxes (Jiang et al., 2022; Hu et al.,  
92 2023). However, its specific role in nutrient loading and eutrophication remains poorly understood.  
93 Heiwawu Oxbow Lake (HW lake), situated along a former Yangtze River channel, provides a valuable  
94 setting to examine the temporal dynamics of LGD due to its seasonal hydrological connectivity.  
95 Typically isolated from the Yangtze by November, HW lake experienced an earlier disconnection in  
96 August 2022 due to extreme drought. During this period, the lake's water and nutrient balance  
97 depended almost entirely on precipitation and groundwater, offering an ideal natural experiment to  
98 investigate LGD-driven nutrient loading and eutrophication over a complete hydrological year.

99 In this study, we quantified LGD and its associated nitrogen and phosphorus fluxes by conducting  
100 bi-monthly, high-frequency monitoring of groundwater and lake water levels, and by applying a  $^{222}\text{Rn}$   
101 mass balance model to a typical closed lake in the middle reaches of the Yangtze River. Furthermore,  
102 we examined the influence of meteorological factors on LGD and the dynamic effects of LGD-driven  
103 nutrient inputs on lake trophic status. The results elucidate the role of precipitation and evaporation in  
104 regulating the seasonal dynamics of LGD and highlight the critical influence of LGD on the nutrient  
105 regime of closed lakes. These findings provide a valuable scientific basis for improving water quality  
106 management and mitigating eutrophication in closed-lake systems worldwide.

107

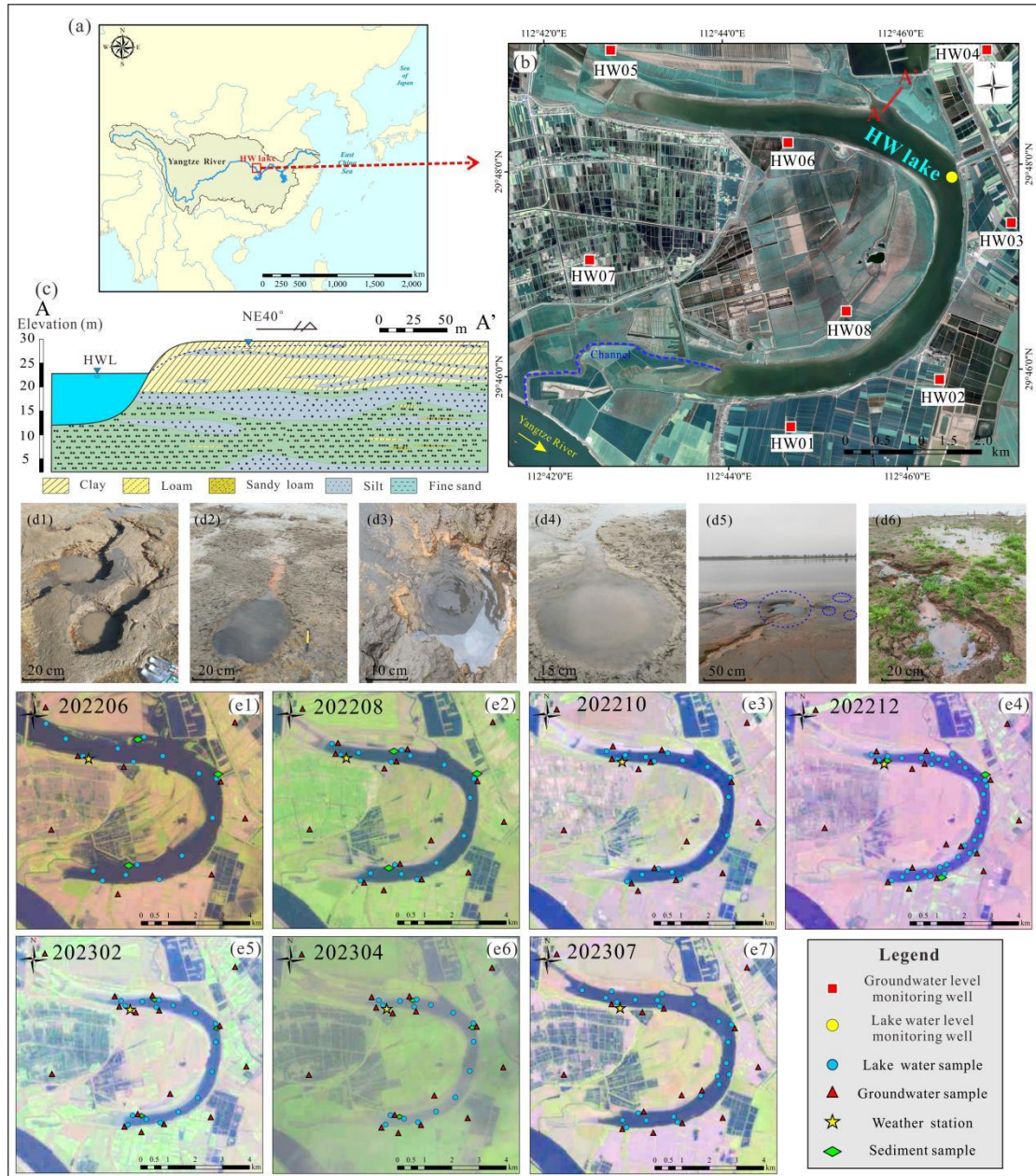
## 108 **2 Materials and Methods**

### 109 **2.1 Study area**

110 HW lake is situated in the southern Jiangnan Plain on the northern bank of the middle reaches of  
111 the Yangtze River, between  $29^{\circ} 45' 10.98'' - 29^{\circ} 48' 52.10''$  N and  $112^{\circ} 41' 35.90'' - 112^{\circ} 46' 32.16''$   
112 E (Figure 1a and b). The region has a subtropical monsoon climate, with an annual mean temperature  
113 of  $15-17^{\circ}\text{C}$ , average annual precipitation of approximately 1400 mm, and average annual evaporation  
114 of approximately 1100 mm (Jia et al., 2015). HW lake was formed in 1967 following the artificial  
115 cutoff of a meander of the Yangtze River, with a downstream channel providing hydrological  
116 connectivity between the lake and the river (Gao et al., 2016). During the wet season, elevated Yangtze  
117 River water levels induce the inflow into HW lake, whereas in the dry season, declining Yangtze River  
118 levels result in backflow from the lake into the river, ultimately leading to complete disconnection. In a  
119 typical hydrological year, HW lake experiences substantial water level fluctuations between the wet  
120 and dry seasons, with a magnitude of up to 8 m.

121 The aquifer interacting with the oxbow lake comprises two distinct layers (Figure 1c). The upper  
122 layer with 5–15 m thickness consists of low-permeability clay and silty clay with a hydraulic  
123 conductivity of approximately  $1 \text{ m}\cdot\text{d}^{-1}$  (Xue et al., 2021). In contrast, the lower layer is a confined  
124 aquifer 50–80 m thick, composed mainly of fine to coarse sand, and exhibits a higher hydraulic  
125 conductivity of approximately  $5\text{--}15 \text{ m}\cdot\text{d}^{-1}$ . Owing to its greater permeability, the lower aquifer  
126 functions as the primary groundwater source directly connected to the lake. Previous studies have  
127 confirmed substantial LGD in HW lake, predominantly occurring as springs (Figure 1 d1–d6) and  
128 seepage flows (Sun et al., 2025b). The area surrounding HW lake is characterized by flat terrain with a  
129 slope of less than 0.1%, and the dominant land use types include forest and farmland. This indicates  
130 that, except for runoff through artificial channels, surface runoff generated by other precipitation is  
131 almost negligible, and the water level gradient, rather than the terrain slope, becomes the key factor  
132 controlling groundwater-lake water exchange.

133 In 2022, a severe drought event in Yangtze River caused the water level of HW lake to decline in  
134 parallel with that of the Yangtze River, ultimately leading to complete disconnection from the river.  
135 Consequently, the lake entered the dry season approximately two months earlier than that in a typical  
136 hydrological year. During the groundwater discharge period, the water level of HW lake was minimally  
137 affected by hydrological fluctuations in the Yangtze River and was instead primarily controlled by  
138 meteorological factors such as precipitation and evaporation.



139  
 140 **Figure 1.** Overview of the study area. (a) Geographical location of the HW lake (study area marked by a red box,  
 141 from Esri). (b) satellite image of HW lake (from Google Earth 2022). (c) Hydrogeological cross-section along  
 142 profile A–A' (profile location indicated by line A–A' in b). The cross-section shows only the upper part of the  
 143 confined aquifer that interacts with the lake, and does not display the full thickness of the aquifer. (d1–d6) Zones  
 144 of concentrated LGD phenomena in HW lake, primarily manifested as spring outlets. (e1–e7) Spatial distribution  
 145 of field sampling sites collected between June and July 2022 (from Landsat 8). The numbers in the figure indicate  
 146 the sampling periods. For example, 202208 represents August 2022. In June 2022 and July 2023, HW lake was  
 147 connected to the Yangtze River through a channel, receiving inflow from the river, which led to higher water levels  
 148 and an expanded inundated area. In the other months, HW lake was isolated from the Yangtze River, representing  
 149 the period when LGD occurred.

150  
 151 **2.2 Field work and laboratory analysis**

152 Systematic field sampling was conducted from June 2022 to July 2023, with a sampling frequency

153 of once every two months. Except for the July 2023 sampling conducted in early July, all other  
 154 campaigns were performed at the end of the even-numbered months. Except for the campaigns in June  
 155 2022, December 2022, and July 2023, all sessions followed a standardized protocol involving the  
 156 collection of 16 lake water samples, 8 well water samples, and 8 pore water samples. A total of 241  
 157 samples were collected (Table 1, Figure 1 e1–e7), comprising 135 lake water samples, 56 well water  
 158 samples, and 50 pore water samples. In addition to sample collection, each campaign included  
 159 simultaneous measurements of environmental parameters, such as groundwater level, lake water level,  
 160 lake depth, and wind speed. Due to seasonal fluctuations in lake water levels, the shoreline position  
 161 shifted over time, resulting in slight spatial variations in the lakeshore sampling points across  
 162 campaigns. The wind speed was continuously recorded at 15-min intervals using a weather station  
 163 installed on the lakeshore, while the precipitation and evaporation data were sourced from the ECMWF  
 164 reanalysis datasets.

165 **Table 1.** Number of samples per sampling campaign.

Time	Number of lake water samples	Number of well water samples	Number of pore water samples	Total
June 23–29, 2022	16	8	2	26
August 26–30, 2022	16	8	8	32
October 26–31, 2022	16	8	8	32
December 17–30, 2022	35	8	10	53
February 20–25, 2023	16	8	8	32
April 23–27, 2023	16	8	8	32
July 6–14, 2023	20	8	6	34
Total	135	56	50	241

166  
 167 Samples from the lake center were collected by boat at fixed preselected locations. Surface water  
 168 was sampled approximately 0.5 m below the surface using a specialized surface water sampler. The  
 169 groundwater samples were categorized into two types: (1) well water collected from monitoring wells  
 170 located 0.5 to 2.5 km from the lakeshore, with the depths between 15 and 30 m, and (2) spring water  
 171 collected from natural springs situated within 15 m of the shoreline and in shallow lake zones, serving  
 172 as the representative lakeshore pore water. In addition, three nearshore lakebed sediment samples were  
 173 collected for incubation experiments to determine the  $^{222}\text{Rn}$  concentrations. The wind speed was  
 174 continuously recorded at 15-min intervals using a weather station installed on the lakeshore, while the  
 175 precipitation and evaporation data were sourced from the ECMWF reanalysis datasets.

176 For  $^{222}\text{Rn}$  analysis, the water samples were collected in 250 mL or 2.5 L glass bottles using an  
 177 overflow method to eliminate residual air.  $^{222}\text{Rn}$  concentrations were quantified using a RAD7 system

178 (DurrIDGE Company, Inc.) equipped with RAD7-H<sub>2</sub>O and RAD7 Big Bottle accessories. To reduce the  
179 measurement uncertainty in lake water samples, the counting time was extended to 60 min per sample.  
180 All <sup>222</sup>Rn analyses were completed within 24 h of sampling, using the RAD7 aqueous system.

$$181 \quad A_0 = A \times e^{\lambda t} \quad (1)$$

182 where A<sub>0</sub> represents the <sup>222</sup>Rn concentration (Bq·m<sup>-3</sup>) at the sampling time; A represents the <sup>222</sup>Rn  
183 concentration (Bq·m<sup>-3</sup>) at the measurement time; λ represents the decay coefficient of <sup>222</sup>Rn, 0.181 d<sup>-1</sup>;  
184 and t represents the time interval (d) between sampling and measurement. The uncertainty in <sup>222</sup>Rn  
185 testing for lake water was approximately 35%, and the uncertainty in <sup>222</sup>Rn testing for groundwater is  
186 approximately 25%.

187 The samples for total nitrogen (TN) and total phosphorus (TP) analysis were field-filtered using a  
188 0.45 μm membrane filter and then stored in 30 mL polyethylene bottles and 20 mL brown screw-cap  
189 glass bottles, respectively. The TP samples were acidified with concentrated HNO<sub>3</sub> to a pH below 2,  
190 sealed, and subsequently analyzed using an inductively coupled plasma optical emission spectrometer  
191 (ICP-OES, iCAP 6000 series, Thermo Fisher Scientific, USA) at the School of Environmental Studies,  
192 China University of Geosciences (Wuhan), with a detection limit of 0.001 mg·L<sup>-1</sup>. TN samples were  
193 analyzed using a total organic carbon/nitrogen analyzer at the Wuhan Botanical Garden, Chinese  
194 Academy of Sciences, with a detection limit of 0.01 mg·L<sup>-1</sup>. Chl *a* concentrations were determined  
195 immediately after sampling using an AquaFluor fluorometer, with a detection limit of 0.5 μg·L<sup>-1</sup>.  
196 Water quality parameters, including pH, temperature, DO, ORP, and EC, were measured in situ using a  
197 HACH-HQ40D multi-parameter probe.

198

### 199 **2.3. <sup>222</sup>Rn mass balance model**

200 In recent years, <sup>222</sup>Rn has been widely used in studies of LGD. Derived from its parent isotope  
201 <sup>226</sup>Ra, <sup>222</sup>Rn has a half-life of 3.82 d. By treating lake water as a closed system, a mass balance model  
202 was developed based on both the sources and sinks of <sup>222</sup>Rn. The <sup>222</sup>Rn flux from the groundwater  
203 discharge was inferred as an unknown term (Schmidt et al., 2010; Luo et al., 2018; Adyasari et al.,  
204 2023). The <sup>222</sup>Rn mass balance model is expressed as follows, and a conceptual diagram of its budget  
205 terms is shown in Figure S1:

$$206 \quad \frac{\partial I^{222}Rn}{\partial t} = F_g + F_d + I^{226}Ra \times \lambda^{226}Ra - F_a - I^{222}Rn \times \lambda^{222}Rn \quad (2)$$

207 where  $F_g$ ,  $F_d$ , and  $F_a$  are the  $^{222}\text{Rn}$  fluxes ( $\text{Bq}\cdot\text{m}^{-2}\cdot\text{d}^{-1}$ ) of groundwater discharge, sediment diffusion, and  
 208 atmospheric escape, respectively;  $I^{226}\text{Ra}$  and  $I^{222}\text{Rn}$  are the pools of  $^{226}\text{Ra}$  and  $^{222}\text{Rn}$  in the lake water  
 209 ( $\text{Bq}\cdot\text{m}^{-2}$ ), which are equal to the concentrations of  $^{226}\text{Ra}$  and  $^{222}\text{Rn}$  multiplied by the water depth; and  
 210 the decay coefficients of  $^{222}\text{Rn}$  ( $\lambda^{222}\text{Rn}$ ) and  $^{226}\text{Ra}$  ( $\lambda^{226}\text{Ra}$ ) were  $0.181\text{ d}^{-1}$  and  $1.31 \times 10^{-11}\text{ d}^{-1}$ ,  
 211 respectively. The measurement times before and after sampling were the first day and the last day of  
 212 the sampling period, respectively. Since there is almost no difference in the lake water level and  $^{222}\text{Rn}$   
 213 concentration at the same location before and after sampling, the change in the  $^{222}\text{Rn}$  in lake water on  
 214 the left side of the equation can be approximated as 0 (Kluge et al., 2007).

215 The  $^{222}\text{Rn}$  flux diffused from the sediment to the lake is one source of the  $^{222}\text{Rn}$  mass balance  
 216 model, and it is calculated by the following formula:

$$217 \quad F_d = \sqrt{(\lambda^{222}\text{Rn} \times n D_m)} (C_p - C_w) \quad (3)$$

218 where  $C_p$  ( $\text{Bq}\cdot\text{m}^{-3}$ ) and  $C_w$  ( $\text{Bq}\cdot\text{m}^{-3}$ ) are  $^{222}\text{Rn}$  concentrations of pore water in sediments and overlying  
 219 lake water, respectively;  $D_m$  ( $\text{cm}^2\cdot\text{s}^{-1}$ ) is the  $^{222}\text{Rn}$  molecular diffusion coefficient in wet bulk sediment;  
 220  $n$  is the porosity of the sediment.

221 To determine the  $^{222}\text{Rn}$  concentrations in sediment pore water, a sediment equilibrium incubation  
 222 experiment was carried out following the procedure proposed by Corbett et al. (1998). The  $D_m$  is  
 223 expressed as:

$$224 \quad -\log D_m = \left( \frac{980}{T_w + 273} \right) + 1.59 \quad (4)$$

225 where  $T_w$  is water temperature ( $^{\circ}\text{C}$ ). An equilibrium incubation experiment with lakebed sediments was  
 226 carried out to obtain the  $^{222}\text{Rn}$  concentration in sediment pore water (Corbett et al., 1998).

227 The atmospheric loss of  $^{222}\text{Rn}$  is estimated based on the following empirical equation, which is  
 228 related to temperature and wind speed (MacIntyre et al., 1995):

$$229 \quad F_a = K (C_w - \alpha C_a) \quad (5)$$

230 where  $K$  values are in  $\text{cm h}^{-1}$  but have been scaled to  $\text{m}\cdot\text{d}^{-1}$  for input into Eq. (5);  $C_w$  is the  
 231 concentration of lake water  $^{222}\text{Rn}$  ( $\text{Bq}\cdot\text{m}^{-3}$ );  $C_a$  is the concentration of  $^{222}\text{Rn}$  in the air ( $\text{Bq}\cdot\text{m}^{-3}$ );  $\alpha$  is the  
 232 gas distribution coefficient (dimensionless) and is a temperature dependent function;  $^{222}\text{Rn}$  from the  
 233 decay of dissolved  $^{226}\text{Ra}$  can be generally omitted for  $^{222}\text{Rn}$  mass balance model.

234 The LGD rate can be obtained by dividing the  $^{222}\text{Rn}$  flux from groundwater discharge by the  $^{222}\text{Rn}$

235 concentration of surrounding groundwater. The formula is as follows (Luo et al., 2018; Wang et al.,  
236 2019):

237 
$$V = \frac{F_g}{C_g} \times 1000 \quad (6)$$

238 where V is the average LGD rate (mm·d<sup>-1</sup>); F<sub>g</sub> is the <sup>222</sup>Rn flux of groundwater discharge  
239 (Bq·m<sup>-2</sup>·d<sup>-1</sup>) ; C<sub>g</sub> is the <sup>222</sup>Rn concentrations in groundwater end member (Bq·m<sup>-3</sup>). A more detailed  
240 description can be found in Section 1 of the SI.

241

## 242 **3 Results and Discussion**

### 243 **3.1 Seasonal variations in LGD rates**

#### 244 **3.1.1 Identification of seasonal variations in LGD**

##### 245 1. Lake water and groundwater level

246 The fluctuations in lake water levels and groundwater levels reflect a pronounced interaction  
247 between groundwater and the lake. During the field monitoring period, both exhibited significant  
248 changes in water level.

249 From June 2022 to July 2023, the lake water level fluctuated significantly between 22.30 and  
250 32.90 m, with a peak in late June 2022 and a low in late February 2023, demonstrating a variation of  
251 10.6 m (Figure 2a). Initially, the HW lake's high water level was sustained by its connection to the  
252 Yangtze River, which was at a high level in June 2022. However, a severe drought from August to  
253 September 2022 caused a rapid decline in the Yangtze River level, resulting in a corresponding  
254 decrease in the HW lake level. From late October 2022 to early May 2023, as the Yangtze River fell  
255 below 26.5 m, HW lake became hydrologically isolated, with no surface water inflow or outflow. The  
256 rate of water level decline slowed from October 2022 to February 2023 and began to rise in March  
257 2023 because of increased precipitation. In May 2023, when the Yangtze River exceeded 26.5 m again,  
258 the HW lake level rose sharply due to the inflow.

259 The groundwater levels from the eight surrounding wells exhibited similar fluctuations, ranging  
260 from 26.6 to 30.9 m (Figure 2a). From June 2022 to April 2023, groundwater levels consistently  
261 declined, with a slight increase observed from April to July 2023. Generally, the groundwater level  
262 trends mirrored those of the lake, except for the period from February to April 2023, when the  
263 groundwater levels decreased while the lake levels increased. The difference between the average  
264 groundwater and lake levels ranged from -1.98 to 4.45 m, affecting the LGD rates over time. In June

265 2022, all eight wells had groundwater levels lower than those of the lake, indicating complete lake  
266 recharge. By July 2023, four wells presented lower groundwater levels, whereas four exhibited higher  
267 levels, suggesting simultaneous recharge and discharge. From August 2022 to April 2023, groundwater  
268 consistently discharged into the lake, with the largest groundwater-lake level difference occurring in  
269 December 2022, indicating the highest LGD rate during that period (Figure 2b).

270

## 271 2. Lake water and groundwater $^{222}\text{Rn}$ concentration

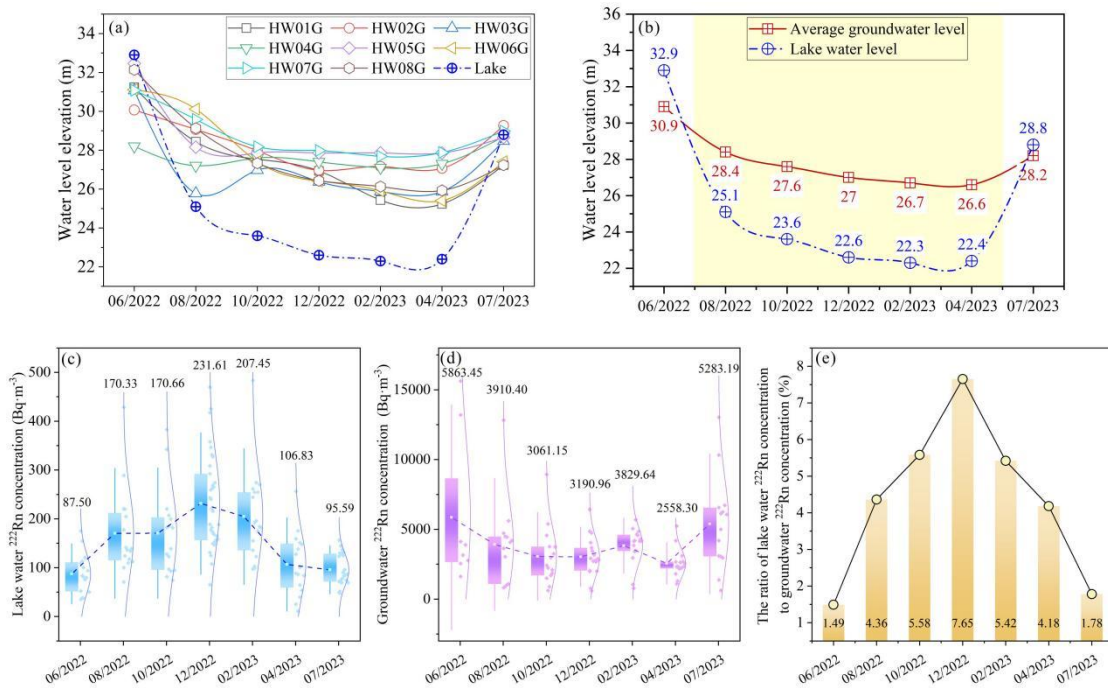
272 As a limited tracer for LGD, the concentration of  $^{222}\text{Rn}$  can indicate changes in LGD. During the  
273 field monitoring period, both lake water and groundwater concentrations underwent some variations,  
274 with differing magnitudes.

275 The fluctuation in the lake water  $^{222}\text{Rn}$  concentration from June 2022 to July 2023 (Figure 2c)  
276 exhibited an initial increase followed by a decrease. The lowest concentration occurred in June 2022,  
277 whereas the highest was recorded in December 2022, with values of 87.50 and 231.61  $\text{Bq}\cdot\text{m}^{-3}$ ,  
278 respectively. Similarly, groundwater also demonstrated a trend of initial decrease followed by an  
279 increase (Figure 2d), with the highest values in June 2022 and the lowest values in April 2023, at  
280 5863.45 and 2558.30  $\text{Bq}\cdot\text{m}^{-3}$  respectively.

281 During the period of groundwater discharge to the lake, when groundwater levels were  
282 consistently above lake levels (August 2022 to April 2023), the lake water  $^{222}\text{Rn}$  concentration ranged  
283 from 106.83 to 231.61  $\text{Bq}\cdot\text{m}^{-3}$ . While, the groundwater  $^{222}\text{Rn}$  concentration ranged from 2558.30 to  
284 3910.40  $\text{Bq}\cdot\text{m}^{-3}$ . Based on the coefficient of variation (CV, used to measure the relative dispersion of  
285 data, defined as the ratio of the standard deviation to the arithmetic mean), the  $^{222}\text{Rn}$  concentration in  
286 groundwater (CV  $\approx$  17.60%) is more stable than that in lake water (CV  $\approx$  26.62%), indicating a  
287 relatively consistent  $^{222}\text{Rn}$  endmember value for groundwater. Because groundwater was the primary  
288 source of  $^{222}\text{Rn}$  in the lake, variations in lake water  $^{222}\text{Rn}$  concentrations reflected changes in the LGD  
289 rate. As shown in Figure 2e, the ratio of lake water to groundwater  $^{222}\text{Rn}$  concentration initially  
290 increased and then decreased with a peak in December 2022, which suggested that the LGD rate was  
291 the highest during that period. This pattern is consistent with the relationship between groundwater and  
292 lake water levels.

293 Notably, as shown in Figure. 2a and c, during the two periods when the groundwater level was  
294 lower than the lake water level (June 2022 and July 2023), lake-water  $^{222}\text{Rn}$  concentrations were 87.50

295 and 95.59 Bq m<sup>-3</sup>, respectively, which are lower than those in the other periods, indicating that  
 296 groundwater discharge was generally limited. Nevertheless, measurable <sup>222</sup>Rn was still detected in the  
 297 lake water, suggesting additional inputs from other water sources. Concurrently, <sup>222</sup>Rn concentrations in  
 298 the Yangtze River were 90.50 and 50.47 Bq m<sup>-3</sup>, respectively. In June 2022, the lake-water <sup>222</sup>Rn  
 299 concentration was very similar to that of the Yangtze River, indicating that the lake was mainly  
 300 controlled by Yangtze River inputs during this period. In contrast, in July 2023 the lake-water <sup>222</sup>Rn  
 301 concentration was slightly higher than that of the Yangtze River; together with the observation that  
 302 groundwater levels in some monitoring wells were still slightly higher than the lake level, this suggests  
 303 the presence of weak, localized groundwater discharge during this period. In addition, intense summer  
 304 precipitation led to increased catchment runoff into the lake, which generally exhibited high <sup>222</sup>Rn  
 305 concentrations, primarily derived from <sup>222</sup>Rn released through interactions between rainfall and surface  
 306 soils rather than from aquifer groundwater. Overall, the higher lake-water <sup>222</sup>Rn concentration in July  
 307 2023 compared with June 2022 reflects the combined effects of Yangtze River input, localized weak  
 308 groundwater discharge, and precipitation-driven runoff.



309 **Figure 2.** (a) Variations in lake water level and groundwater levels across all groundwater monitoring points. (b)  
 310 Variations in lake water levels compared with the average groundwater level, the yellow area indicates the period  
 311 of LGD. (c) Variations in the lake water concentrations of <sup>222</sup>Rn. (d) Variations in the groundwater concentrations  
 312 of <sup>222</sup>Rn. In (c) and (d), the top and bottom of each box represent the 75th and 25th percentiles of the data,  
 313 respectively; the ends of the whiskers indicate the maximum and minimum values within 1.5 times the  
 314 interquartile range; the small white square inside the box denotes the mean; the side curves illustrate the data's  
 315 dispersion and distribution pattern; the dark blue dashed line connects the mean values across different periods. (e)  
 316 Variations in the ratio of <sup>222</sup>Rn concentrations in lake water to groundwater.  
 317  
 318

319 **3.1.2 Quantification of LGD rates for each period**

320 Based on the lake level and groundwater monitoring data, the period from late August 2022 to late  
 321 April 2023 was characterized by consistently higher groundwater levels than the lake stage, during  
 322 which the lake was hydrologically isolated from external surface water inputs. This interval was  
 323 conservatively defined as the active phase of LGD (Figure 2b). Using the  $^{222}\text{Rn}$  mass balance model,  
 324 LGD rates were computed for each period of groundwater discharge during groundwater excretion.

325 Table 2 summarizes the detailed parameters and results for the source and sink terms across each  
 326 sampling period. A comparison of the  $^{222}\text{Rn}$  fluxes associated with the source and sink terms in the  
 327  $^{222}\text{Rn}$  mass balance model for each period is shown in Figure S2. In terms of source, the  
 328 groundwater-derived  $^{222}\text{Rn}$  input flux ranged from  $90.48 \pm 36.32$  to  $165.02 \pm 63.09$   $\text{Bq}\cdot\text{m}^{-2}\cdot\text{d}^{-1}$ , while  
 329 the diffusive flux of  $^{222}\text{Rn}$  from sediment pore water varied between  $18.82 \pm 2.88$  and  $21.51 \pm 3.29$   
 330  $\text{Bq}\cdot\text{m}^{-2}\cdot\text{d}^{-1}$ . In terms of sink, the radioactive decay flux of  $^{222}\text{Rn}$  in lake water ranged from  $73.47 \pm$   
 331  $26.74$  to  $163.49 \pm 59.51$   $\text{Bq}\cdot\text{m}^{-2}\cdot\text{d}^{-1}$ , and atmospheric evasion accounted for a flux of  $20.34 \pm 6.46$  to  
 332  $38.51 \pm 12.87$   $\text{Bq}\cdot\text{m}^{-2}\cdot\text{d}^{-1}$ .

333 The LGD rates for each period were calculated by dividing the flux of  $^{222}\text{Rn}$  input from LGD by  
 334 the corresponding groundwater  $^{222}\text{Rn}$  concentration (Figure 3a). From August 2022 to April 2023, the  
 335 LGD rates ranged from  $35.36 \pm 16.39$  to  $51.71 \pm 23.23$   $\text{mm}\cdot\text{d}^{-1}$ , with the maximum value being 1.46  
 336 times the minimum value. Notably, an increasing trend in groundwater excretion rates was observed  
 337 from August 2022 to December 2022, which was followed by a decreasing trend from December 2022  
 338 to April 2023. The highest rate of groundwater excretion occurred in December 2022, whereas the  
 339 lowest LGD rate was recorded in April 2023.

340 **Table 2.** The calculation parameters and results of the  $^{222}\text{Rn}$  mass balance model for each period.

	08/2022	10/2022	12/2022	02/2023	04/2023
Lake water $^{222}\text{Rn}$ concentration ( $\text{Bq}\cdot\text{m}^{-3}$ )	$170.33 \pm 88.71$	$170.66 \pm 89.10$	$231.61 \pm 96.53$	$207.45 \pm 98.16$	$106.83 \pm 63.85$
Air $^{222}\text{Rn}$ concentration ( $\text{Bq}\cdot\text{m}^{-3}$ )	16.20	16.20	16.20	16.20	16.20
Wind speed above 2 m lake surface ( $\text{m}\cdot\text{s}^{-1}$ )	$1.48 \pm 0.82$	$1.37 \pm 0.83$	$1.08 \pm 1.11$	$1.65 \pm 1.44$	$2.05 \pm 1.57$
K ( $\text{m}\cdot\text{d}^{-1}$ )	$0.30 \pm 0.02$	$0.17 \pm 0.01$	$0.08 \pm 0.01$	$0.16 \pm 0.01$	$0.34 \pm 0.01$
Sc	554.34	937.71	1572.2	1492.73	871.45
Lake water temperature ( $^{\circ}\text{C}$ )	29.19	18.43	8.86	9.78	19.89
Lake water depth (m)	4.9	4.2	3.9	3.8	3.8
Groundwater $^{222}\text{Rn}$ concentration ( $\text{Bq}\cdot\text{m}^{-3}$ )	$3910.40 \pm 3511.38$	$3061.15 \pm 2099.00$	$3028.17 \pm 1412.72$	$3829.64 \pm 1316.67$	$2588.30 \pm 998.11$
The $^{222}\text{Rn}$ flux of atmospheric escape	$49.80 \pm 18.20$	$30.96 \pm 10.27$	$20.34 \pm 6.46$	$37.12 \pm 11.56$	$38.51 \pm 12.87$

	(Bq·m <sup>-2</sup> ·d <sup>-1</sup> )				
The <sup>222</sup> Rn flux of pore in sediment diffusion (Bq·m <sup>-2</sup> ·d <sup>-1</sup> )	24.70±3.78	21.10 ± 3.23	18.82±2.88	18.74±2.87	21.51±3.29
The <sup>222</sup> Rn flux of decay (Bq·m <sup>-2</sup> ·d <sup>-1</sup> )	151.07± 54.99	129.74±47.22	163.49±59.51	142.68±51.93	73.47±26.74
The <sup>222</sup> Rn flux of groundwater discharge (Bq·m <sup>-2</sup> ·d <sup>-1</sup> )	176.16± 58.05	139.59±48.44	165.02± 63.09	161.06±60.63	90.48±36.32
LGDrate (mm·d <sup>-1</sup> )	45.05± 18.39	45.60± 34.20	51.71±23.23	42.06±18.60	35.36±16.39

341

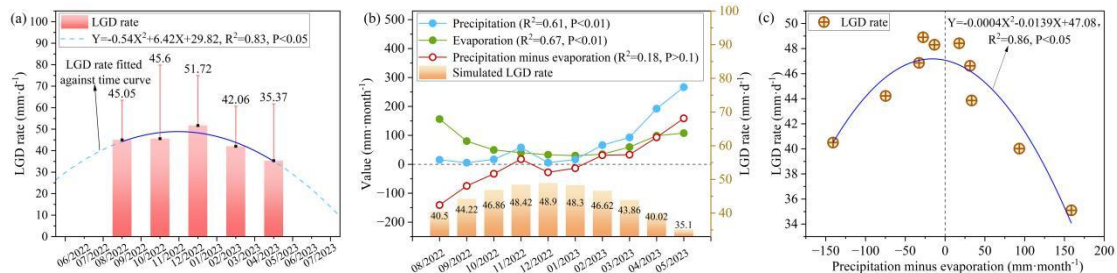
## 342 3.2 Climatic controls on seasonal variations in LGD rates

### 343 3.2.1 Relationship between precipitation and evaporation and LGD rates

344 To obtain a **high-frequency** within the hydrological year, fitting equations were established to  
 345 simulate the monthly LGD rates during groundwater discharge periods. The quadratic equation  
 346 representing LGD rates based on the <sup>222</sup>Rn mass balance model and time was  $Y = -0.54X^2 + 6.42X +$   
 347  $29.82$ ,  $R^2 = 0.83$ ,  $P < 0.05$  (where X represents the time and Y represents the LGD rate) (Figure 3a).  
 348 Due to the small sample size, the robustness of the model's fit may be limited. Nonetheless, under the  
 349 field observed conditions, the monthly fluctuations of lake and groundwater levels were relatively  
 350 small and exhibited regular patterns, so the actual monthly variation of LGD showed a predictable  
 351 "increase followed by decrease" pattern. Therefore, the predictions of this model are considered  
 352 reliable. Using this equation, the LGD rates were estimated for the period from August 2022 to May  
 353 2023. Although the water level at the Jianli station of the Yangtze River exceeded 26.5 m in May 2023  
 354 for just 10 d, the inflow from the Yangtze River to the HW lake was minimal and insufficient to raise  
 355 the lake level above the groundwater level. Therefore, groundwater discharge into the lake continued in  
 356 May 2023. The simulated LGD rates ranged from 35.10 to 48.90 mm·d<sup>-1</sup> between August 2022 and  
 357 May 2023 (Figure 3b), with an approximately 8% error compared to the rates derived from the <sup>222</sup>Rn  
 358 mass balance model. These rates exhibited an increasing trend followed by a decreasing trend, peaking  
 359 in the middle of the groundwater discharge period, and tapering at both the beginning and end stages.

360 During the groundwater discharge period, the changes in precipitation and evaporation were  
 361 inversely related to the changes in LGD, demonstrating a clear negative correlation with LGD rates,  
 362 with correlation coefficients of  $R^2=0.61$ ,  $P < 0.01$  and  $R^2=0.67$ ,  $P < 0.01$ , respectively (Figure 3b,  
 363 Figure S3 a and b). This suggested that lower monthly precipitation and evaporation contributed to the  
 364 larger LGD. This aligns with Jiang et al.'s (2024) results showing an inverse relationship between LGD  
 365 rates and precipitation/evaporation. Additionally, the value of precipitation minus evaporation (PME)

366 played a significant role in the hydrological cycle. By analyzing the relationship between the PME and  
 367 LGD rates, a non-linear relationship was identified, with the fitted equation being  
 368  $Y=-0.0004X^2-0.0139X+47.08$ ,  $R^2=0.86$ ,  $P<0.05$  (Figure 3c). When PME was greater than 0, a larger  
 369 PME resulted in a smaller LGD. When PME was less than 0, a smaller PME led to a smaller LGD.  
 370 When both precipitation and evaporation were low and the PME approached 0, LGD reached its  
 371 maximum value.



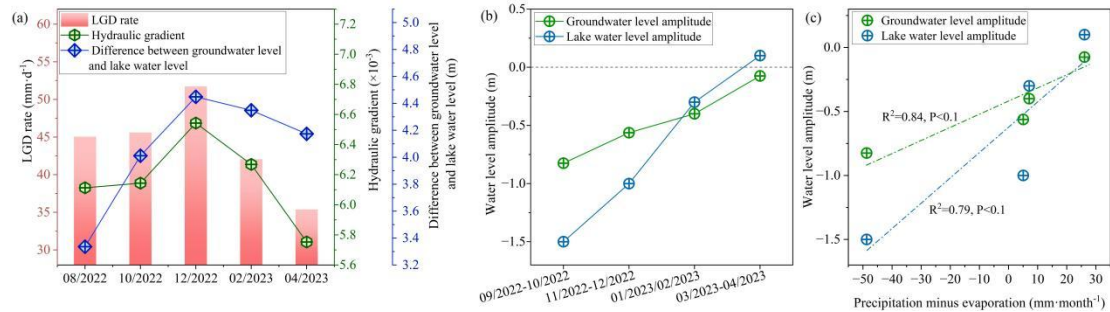
372  
 373 **Figure 3.** (a) The LGD rate of different periods and their fitted relationship between LGD rate and time. (b)  
 374 Relationship between simulated LGD rate and precipitation and evaporation, where  $R^2$  represents the linear  
 375 correlation coefficient between this indicator and the LGD rate. (c) Relationship between PME and LGD rate.  
 376

### 377 3.2.2 Dominance of precipitation and evaporation on seasonal variations in LGD rates

378 **The hydraulic gradient determines the variation in the LGD rate.** At different periods, a strong  
 379 correlation was observed between the LGD rate and hydraulic gradient ( $R^2=0.77$ ,  $P<0.05$ ) (Figure 4a),  
 380 with both showing a consistent trend of change, in accordance with Darcy's law (Tecklenburg and  
 381 Blume; 2017) (Figure 4a). The hydraulic gradient is controlled by the water level difference between  
 382 groundwater and lake water—when this difference increases, the LGD rate rises; when it decreases, the  
 383 LGD rate declines. From August to December 2022, the water level difference increased, leading to a  
 384 rising LGD rate; from December 2022 to April 2023, the difference decreased, resulting in a lower  
 385 LGD rate (Figure 4a). This variation is determined by the differences in groundwater level and lake  
 386 water level. If the lake level drops more than the groundwater level, the gradient increases and LGD  
 387 intensifies; if the groundwater level drops more, the gradient and LGD both decline (Figure 4b).

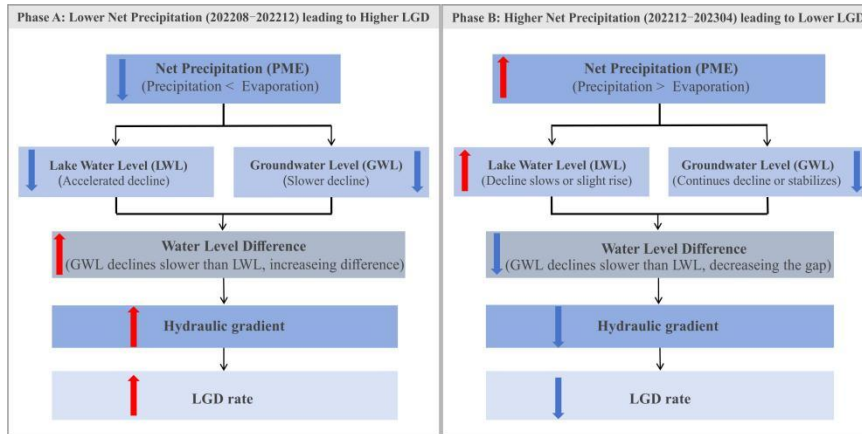
388 Monitoring data show that lake levels consistently declined during the study period, though the  
 389 rate of decline slowed, primarily due to low precipitation, reduced evaporation, cooler temperatures,  
 390 and decreased water consumption by agriculture and aquatic organisms. After February 2023,  
 391 increasing precipitation slightly raised lake levels. Groundwater levels also declined steadily, mainly  
 392 due to continuous LGD to lake, with minimal influence from human extraction or evaporation.  
 393 Between August and December 2022, groundwater levels fell more slowly than lake levels, increasing

394 the hydraulic gradient and LGD. From February 2023 onward, the groundwater level declined more  
 395 than the lake level, reducing the gradient and LGD rate. By April 2023, groundwater levels stabilized  
 396 while lake levels rose slightly, further decreasing the hydraulic gradient and LGD.



397  
 398 **Figure 4.** (a) Temporal characteristics of LGD rate, hydraulic gradient, and difference in groundwater and lake  
 399 water levels. (b) Temporal characteristics of groundwater and lake water level change amplitudes, negative values  
 400 indicate the amplitudes of water level decline, while positive values represent the amplitudes of water level rise. (c)  
 401 Relationship between groundwater level amplitude, lake water level amplitude, and PME.  
 402

403 Net precipitation (PME) indirectly controls seasonal variations in LGD by regulating the hydraulic  
 404 gradient. Observations show that PME is closely associated with lake water level variations. During  
 405 periods of higher PME, the decline in lake water level slows or even reverses, whereas under lower  
 406 PME conditions, the rate of lake level decline accelerates. Meanwhile, groundwater levels exhibit a  
 407 response pattern consistent with lake water level variations. From a mechanistic perspective, this  
 408 relationship can be explained as follows: PME directly influences lake water level dynamics by  
 409 regulating the lake water balance, and further alters the water level difference between the lake and  
 410 groundwater. When the decline in lake water level is relatively small, groundwater discharge to the lake  
 411 weakens, thereby suppressing the decline in groundwater levels. Conversely, when lake level decline  
 412 intensifies, groundwater discharge is enhanced, leading to a further decrease in groundwater levels.  
 413 Ultimately, this process regulates the seasonal variability of LGD rates by modifying the hydraulic  
 414 gradient. On this basis, this process can be conceptualized as a coupled framework of “meteorological  
 415 forcing–water level response–hydraulic gradient regulation–LGD variation” (Figure. 5).



416  
 417 **Figure 5.** Conceptual model illustrating the mechanisms by which precipitation and evaporation influence LGD  
 418 rates. Red upward arrows and blue downward arrows indicate increasing and decreasing trends of the  
 419 corresponding parameters, respectively.  
 420

421 **3.3 Impact of LGD-carried N and P on seasonal nutrient status of lakes**

422 **3.3.1 Seasonal variations in TN and TP loads carried by LGD**

423 Between August 2022 and April 2023, the concentration of TN in the groundwater exhibited  
 424 notable temporal variability, ranging from 0.24 to 0.46 mmol·L<sup>-1</sup>. The lowest concentration was  
 425 observed in August 2022, whereas the peak was observed in December 2022 (Table 3). In comparison,  
 426 the range of temporal variations in TP concentration in groundwater was wider, spanning from 6.46 ×  
 427 10<sup>-3</sup> to 2.19 × 10<sup>-2</sup> mmol·L<sup>-1</sup> (Table 3). The lowest TP concentration was recorded in December 2022,  
 428 whereas the highest occurred in February 2023. Based on Eh, DO, and EC results (Table S3), TP  
 429 concentration fluctuations likely result from the combined effects of internal adsorption and fixation,  
 430 external input pulses, and geochemical competition under the background of an oxidation-enhanced  
 431 environment driven by declining water levels (Eh and DO continuously increasing). For a detailed  
 432 analysis, see the SI.

433 **Table 3.** Concentrations of TN and TP in groundwater at various periods and loads of TN and TP carried by LGD.

	TN concentration in groundwater (mmol·L <sup>-1</sup> )	TP concentration in groundwater (mmol·L <sup>-1</sup> )	LGD-TN (mmol·m <sup>-2</sup> ·d <sup>-1</sup> )	LGD-TP (mmol·m <sup>-2</sup> ·d <sup>-1</sup> )
08/2022	0.24	1.69×10 <sup>-2</sup>	10.76	0.76
10/2022	0.33	2.00×10 <sup>-2</sup>	15.22	0.91
12/2022	0.46	6.46×10 <sup>-3</sup>	24.00	0.33
02/2023	0.34	2.19×10 <sup>-2</sup>	14.25	0.92
04/2023	0.39	8.24×10 <sup>-3</sup>	13.93	0.29

434  
 435 Multiplying the LGD rate by the concentrations of TN and TP in the groundwater demonstrated  
 436 the nutrient load carried by LGD. The variations in nutrient loads from August 2022 to April 2023 are  
 437 shown in Figures 6d and 6e. The loads of TN carried by LGD (LGD-TN) ranged from 10.76 to 24.00  
 438 mmol·m<sup>-2</sup>·d<sup>-1</sup>, with the lowest load occurring in August 2022 and the highest in December 2022.

439 Similarly, the loads of TP carried by LGD (LGD-TP) ranged from 0.29 to 0.92  $\text{mmol}\cdot\text{m}^{-2}\cdot\text{d}^{-1}$ , with the  
440 highest load observed in December 2022 and the lowest in April 2023. The temporal variation in  
441 LGD-TN loads followed the trend of the LGD rate and was primarily influenced by the LGD rate. In  
442 contrast, the variation in LGD-TP loads over time did not align with the LGD rate and was mainly  
443 controlled by the concentration of TP in the groundwater.

444

### 445 **3.3.2 Seasonal relationship between LGD-carried TN/TP loads and nutrient status of lakes**

446 The nutrient status of lakes is determined by various parameters, and the concentration of Chl *a* in  
447 lake water is considered particularly important. In this study, no significant correlation was observed  
448 between Chl *a* concentration and the concentrations of TN and TP (Figures 6a and 6b). However, a  
449 correlation was identified with the TN to TP molar ratio (TN/TP) (Figure 6c). As the TN/TP ratio  
450 approached the Redfield ratio of 16 (Figure 6c), the Chl *a* concentration increased (Redfield, 1960),  
451 whereas a deviation from this ratio was associated with a decrease in Chl *a* concentration, which was  
452 consistent with the findings reported in other studies (Qin et al., 2020).

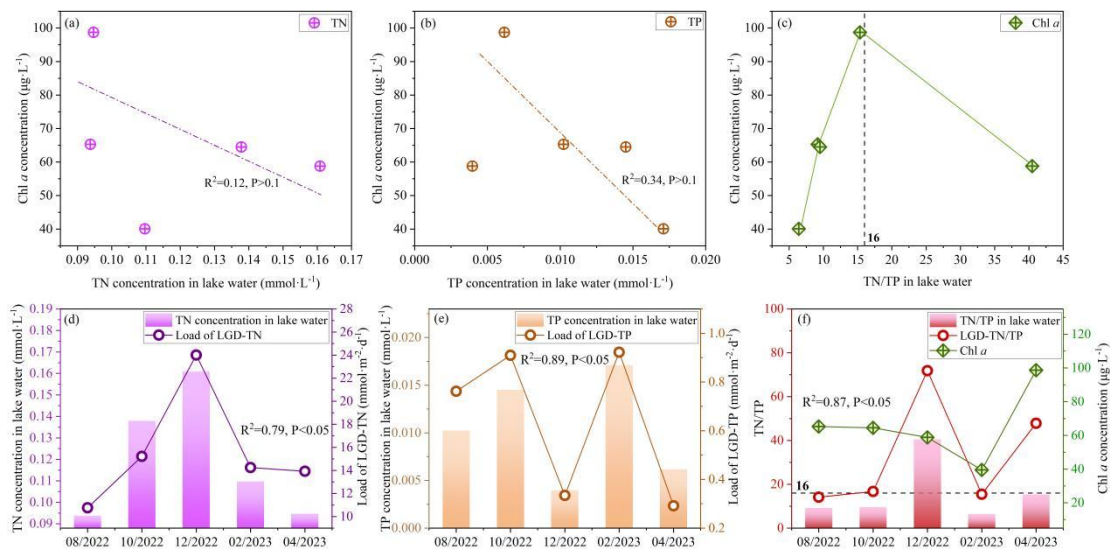
453 In the absence of surface water inflow and pollutant discharge from prohibited human activities, N  
454 and P enter the lake primarily through groundwater discharge, atmospheric deposition, and sediment  
455 release. To quantify TN and TP inputs from atmospheric deposition and sediment release,  
456 comprehensive field monitoring and experimental investigations were conducted during HW lake  
457 periods (Tables S1 and S2). The results indicated that the TN and TP loads from atmospheric deposition  
458 were 0.09 and  $9.68\times 10^{-4}$   $\text{mmol}\cdot\text{m}^{-2}\cdot\text{d}^{-1}$ , respectively. Simultaneously, the diffusive TN and TP loads  
459 from lakebed sediment were 0.08 and  $1.29\times 10^{-4}$   $\text{mmol}\cdot\text{m}^{-2}\cdot\text{d}^{-1}$ , respectively. In contrast, the LGD-TN  
460 and LGD-TP loads were 1–2 orders of magnitude higher than those from atmospheric deposition and  
461 sediment release, indicating that LGD-TN and LGD-TP constituted the primary sources of TN and TP  
462 in the lake. A strong correlation was observed between LGD-TN loads and TN concentrations in lake  
463 water ( $R^2=0.79$ ,  $P<0.05$ ) (Figure 6d), whereas the LGD-TP loads exhibited entirely consistent  
464 variations with TP concentrations in lake water ( $R^2=0.89$ ,  $P<0.05$ ) (Figure 6e), highlighting their  
465 significant influence.

466 The molar ratio of TN to TP in LGD (LGD-TN/TP) exhibited variations that were entirely  
467 consistent with the TN/TP ratio in the lake water, indicating a strong correlation ( $R^2=0.82$ ,  $P<0.05$ )  
468 (Figure 6f), thereby indicating its regulatory effect on the lake water TN/TP ratio. Based on the

469 observed changes in LGD-TN/TP and their reflection in lake water TN/TP, when the lake water TN/TP  
 470 reached 15.35 in April 2023, the Chl *a* concentration was elevated. These results demonstrated that the  
 471 LGD-derived TN and TP substantially influenced the lake's nutrient status by modulating the TN/TP  
 472 ratio, thereby affecting the Chl *a* concentration and the overall nutrient balance.

473 In addition, light availability and water temperature can also affect Chl *a* growth. Although higher  
 474 temperatures and favorable light conditions in summer and autumn are theoretically conducive to  
 475 phytoplankton proliferation, Figure. 6f shows that Chl *a* concentrations decreased continuously from  
 476 August 2022 to February 2023, but increased rapidly and reached a peak in April 2023. This increase  
 477 may be partly related to improvements in light and temperature conditions. However, during the  
 478 summer wet season, when temperature and light are most favorable and LGD is absent, the mean Chl *a*  
 479 concentration was only ~60  $\mu\text{g/L}$ , which is much lower than the 98.69  $\mu\text{g/L}$  observed in April 2023.  
 480 These results suggest that light and temperature are not the dominant drivers of Chl *a* variability;  
 481 instead, nitrogen and phosphorus concentrations and their TN/TP are the key controlling factors.

482 In lake eutrophication management, Chl *a* accumulation is governed not only by the absolute  
 483 concentrations of nitrogen and phosphorus but also by the TN/TP, which determines the dominant type  
 484 of nutrient limitation. Low TN/TP indicate nitrogen limitation, whereas high TN/TP indicate  
 485 phosphorus limitation. Given that present study has shown that groundwater can significantly alter lake  
 486 TN/TP, its influence should be explicitly considered when identifying nutrient limitation mechanisms  
 487 and developing targeted nitrogen and phosphorus reduction strategies.



488 **Figure 6.** Relationship between LGD-TN and TP loads and lake water TN and TP concentrations, as well as the  
 489 lake water Chl *a* concentration. (a) Relationship between Chl *a* concentration and lake water TN concentration. (b)  
 490 Relationship between Chl *a* concentration and lake water TP concentration. (c) Relationship between Chl *a*  
 491 concentration and lake water TN/TP. (d) Relationship between lake water TN concentration and LGD-TN load. (e)  
 492 Relationship between lake water TP concentration and LGD-TP load. (f) Relationship between lake water TN/TP  
 493

and LGD-TN/TP load.

### 3.4 Implications

#### 3.4.1 Advantages of high-frequency observations in LGD research

Traditional low-frequency sampling (e.g., single measurements or quarterly observations) is insufficient to capture short-term variability in LGD and its coupling with transient meteorological conditions and water level fluctuations. In contrast, high-frequency observations enable the resolution of rapid LGD responses to environmental drivers—such as meteorological forcing and water level changes—over shorter timescales. They also provide high-resolution hydrological time series, thereby offering robust data support for more accurate estimation of LGD fluxes.

More importantly, the continuous datasets obtained from high-frequency observations allow this study to reveal several key conceptual insights that cannot be captured by low-frequency sampling. First, LGD responses to meteorological forcing are not simply synchronous, but may exhibit significant lag effects and stage-dependent regulation. Second, the synchronous fluctuations between lake water levels and groundwater levels may follow different dominant control pathways under varying hydrological conditions, thereby highlighting the nonlinear characteristics of the “meteorological forcing → water level response → LGD variation” chain. In addition, the short-term contributions of LGD to lake nutrient inputs and ecological responses (e.g., variations in Chl-a or algal bloom events) can be detected in a timely manner, whereas such signals are often averaged out and obscured in low-frequency observations.

From a management perspective, high-frequency observations allow for a more refined characterization of the instantaneous contribution of LGD to lake nutrient loading and its relationship with eutrophication processes, thereby providing a scientific basis for early warning and refined regulation of lake water quality risks. Meanwhile, LGD predictive models developed based on high-frequency data can significantly improve the ability to capture groundwater input responses under extreme meteorological conditions, offering more timely decision support for lake water resource and ecosystem management.

Therefore, in LGD research, high-frequency observations not only improve the accuracy of flux estimation, but more importantly overcome the temporal limitations of low-frequency sampling, enabling the identification of dynamic mechanisms and ecological effects of LGD processes. As such, they should be prioritized in future research and applications.

525

### 526 **3.4.2 Dominant factors controlling the seasonal variability of LGD**

527 The seasonal variability of LGD is mainly influenced by three categories of  
528 factors—meteorological, hydrological, and anthropogenic—with the dominant controls differing across  
529 lake types.

530 (1) In open lakes (e.g., Poyang Lake and Tonle Sap Lake), hydrological processes are a major  
531 control on LGD dynamics. Their hydraulic connection with external rivers (such as the Yangtze and  
532 Mekong Rivers) causes rapid lake-level rises during the wet season and pronounced declines during the  
533 dry season, thereby modifying the hydraulic gradients between the littoral zone and aquifer and directly  
534 regulating groundwater discharge rates (Burnett et al. 2017; Li et al. 2020). (2) In closed lakes, where  
535 external fluvial influence is minimal, LGD dynamics are strongly influenced by the balance between  
536 precipitation and evaporation. Previous studies (Shi et al., 2022) have shown that under relatively  
537 stable groundwater levels, strong evaporation lowers lake levels, steepens the hydraulic gradient, and  
538 enhances LGD, whereas precipitation-dominated periods raise lake levels and suppress LGD. Hence,  
539 the seasonal oscillation of LGD in closed-basin systems can be interpreted as a periodic adjustment of  
540 lake–groundwater hydraulic connectivity driven by meteorological forcing. (3) Anthropogenic  
541 activities, such as artificial water regulation and groundwater abstraction, can further modify LGD by  
542 altering regional hydrological circulation and the hydraulic relationships between lakes and aquifers  
543 (Xiong et al., 2023).

544

### 545 **3.4.3 Regulatory role of LGD in lake nutrient status**

546 In closed lakes lacking significant surface inflow, LGD not only constitutes a key component of  
547 the water balance but also can play a significant role in nutrient transport and water quality evolution.  
548 The nitrogen and phosphorus fluxes carried by LGD can influence the spatial and temporal patterns of  
549 nutrient concentrations and Chl *a* within the lake. Several studies support this mechanism. For instance,  
550 Xu et al. (2025) showed that in small semi-arid lakes, LGD inputs play a key role in shaping the spatial  
551 distribution of Chl *a*, while Shi et al. (2022) reported a delayed response of lake trophic conditions to  
552 LGD-derived nutrient inputs. Such lakes are typically characterized by strong enclosure and long water  
553 residence times, conditions that can amplify the influence of groundwater in biogeochemical cycling  
554 and ecological processes.

555         Synthesizing current knowledge, the linkage from seasonal forcing to ecological response in  
556 closed lakes can be conceptualized as follows: meteorological conditions (precipitation–evaporation  
557 balance) serve as the initial driver, regulating lake–groundwater hydraulic gradients and **thereby**  
558 **influencing the seasonal magnitude of LGD**. LGD, in turn, **acts as an important conduit** for nutrient  
559 fluxes, with its temporal variability shaping nutrient and Chl *a* distributions and ultimately modulating  
560 nutrient dynamics.

561         Previous studies have long approached the issue of internal nutrient loading in lakes primarily  
562 from the perspective of nitrogen and phosphorus release from bottom sediments, emphasizing the role  
563 of sediment-derived nutrients in shaping lake trophic status (Donohue and Garcia Molinos, 2009). For  
564 lakes where LGD-derived nutrient loads are relatively small during specific seasons, sedimentary  
565 nutrient release can indeed constitute a major source to the overlying water column, consistent with  
566 traditional understanding (Xu et al., 2017). However, in systems where LGD inputs are substantial,  
567 focusing solely on sedimentary release may not fully capture the true structure of lake nutrient sources.  
568 Although systematic studies that simultaneously assess both sediment nutrient release and  
569 LGD-derived inputs remain limited, existing evidence indicates that LGD is likely a key mechanism  
570 sustaining nutrient cycling and ecological succession in closed-basin lakes, highlighting the need for  
571 more comprehensive and quantitative investigations.

572         HW lake and other study cases are all typical closed shallow lakes, with limited exchange between  
573 the lake water and surface inflows, making LGD the primary hydrological input. A large number of  
574 similar lakes exist worldwide (e.g., closed lakes in the North American Great Plains, inland lakes in  
575 Africa and Central Asia), which may also be significantly influenced by LGD. Moreover, the  
576 regulatory effect of LGD on the spatial distribution of nitrogen, phosphorus, Chl *a*, and algal growth is  
577 amplified in lakes with long water residence times and stable sediment–water exchange. Therefore, this  
578 mechanism **is likely applicable to** other closed shallow lakes, particularly those with pronounced  
579 seasonal climates and a high proportion of shallow areas.

580

#### 581         **3.4.4 Future recommendations for the lake management of closed shallow lakes**

582         Based on the above understanding, future research should adopt a systems-based perspective,  
583 focusing on comparative analyses of LGD inputs versus internal sediment release and quantitatively  
584 identifying their relative importance across different lake types and temporal scales **to better constrain**

585 **the dominant nutrient sources**. This approach can provide a scientific basis for designing targeted  
586 nitrogen and phosphorus reduction strategies, as well as effective lake management and ecological  
587 restoration measures, thereby improving water quality and ecological function in closed lakes.

588 Moreover, climate change is expected to modulate these processes. In the East Asian monsoon  
589 region, future precipitation is projected to become more concentrated in summer, while non-summer  
590 periods, particularly autumn and winter, may experience reduced rainfall and increased evaporation.  
591 Because LGD predominantly occurs during non-summer periods, increased net precipitation  
592 (precipitation minus evaporation) could enhance groundwater discharge, **which may lead to increased**  
593 LGD-derived nutrient loads. These considerations further **highlight the important role** of groundwater  
594 in regulating nutrient balances in closed lakes and emphasize the need for future nutrient management  
595 strategies to account for both LGD variability and climate-driven hydrological changes.

596

#### 597 **4 Conclusions**

598 High-frequency monitoring and hydrochemical methods were employed to investigate the  
599 dynamics of LGD and associated nutrient loads in Heiwawu Oxbow Lake from August 2022 to April  
600 2023, revealing the regulatory mechanisms of precipitation-evaporation processes. The LGD flux  
601 exhibited an increasing-then-decreasing trend during the study period, ranging from 35.36 to 51.71  
602  $\text{mm}\cdot\text{d}^{-1}$ , with a peak in December 2022 and a minimum in April 2023. The LGD rates were governed  
603 by the hydraulic gradient between groundwater and lake water, which responded nonlinearly to net  
604 monthly precipitation. Positive net precipitation induced rapid lake recharge, reduced the hydraulic  
605 gradient, and suppressed LGD rates. Conversely, negative net precipitation enhanced  
606 evaporation-driven lake discharge, steepened the hydraulic gradient, and increased LGD rates. When  
607 net precipitation approached zero, a critical hydraulic equilibrium was reached, yielding the highest  
608 LGD rates. The LGD was also a major nutrient pathway, with TN and TP loads significantly correlating  
609 with lake concentrations. The TN/TP ratio of LGD aligned with lake water, influencing phytoplankton  
610 structure and Chl *a* levels. This study reveals the regulatory mechanisms by which LGD is controlled  
611 by the precipitation–evaporation balance at the monthly scale, quantitatively evaluates the impacts of  
612 groundwater-driven nutrient transport on lake eutrophication, and, by reference to related global case  
613 studies, provides environmental protection and management implications from a groundwater  
614 perspective. These findings offer new insights into eutrophication control in closed, shallow lakes, and

615 suggest that the advantages of high-frequency LGD observations should be incorporated into lake  
616 management frameworks, along with the development of targeted control strategies during critical  
617 periods of groundwater–lake interactions.

618

### 619 **Acknowledgments**

620 The research was funded by National Natural Science Foundation of China (Nos. 42422707,  
621 U21A2026), and Fundamental and Interdisciplinary Disciplines Breakthrough Plan of the Ministry of  
622 Education of China (No. JYB2025XDXM911). The authors would like to thank all the reviewers who  
623 participated in the review, as well as MJEdition (www.mjeditor.com) for providing English editing  
624 services during the preparation of this manuscript.

625

### 626 **Declaration of interests**

627 The authors declare that they have no known competing financial interests or personal  
628 relationships.

629

### 630 **Data Availability Statement**

631 Data will be made available on request.

632

### 633 **Author contributions**

634 Writing-review & editing, Writing-original draft, Methodology, Investigation, Data curation: XS.  
635 Writing-review & editing, Resources, Methodology, Funding acquisition: YD. Investigation: HT, JX,  
636 HS, YL. Project administration: YD. Funding acquisition: YG. Resources, Project administration: YW.

637

### 638 **References**

639 Adyasari, D., Dimova, N. T., Dulai, H., Gilfedder, B. S., Cartwright, I., McKenzie, T., and Fuleky, P.:  
640 Radon-222 as a groundwater discharge tracer to surface waters, *Earth-Sci. Rev.*, 238, 104321,  
641 <https://doi.org/10.1016/j.earscirev.2023.104321>, 2023.  
642 Arnoux, M., Gibert-Brunet, E., Barbecot, F., Guillon, S., Gibson, J., and Noret, A.: Interactions  
643 between groundwater and seasonally ice-covered lakes: using water stable isotopes and radon-222  
644 multilayer mass balance models, *Hydrol. Process.*, 31, 2566–2581,  
645 <https://doi.org/10.1002/hyp.11206>, 2017.

646 Burnett, W. C., Wattayakorn, G., Supcharoen, R., Sioudom, K., Kum, V., Chanyotha, S., and  
647 Kritsanuwan, R.: Groundwater discharge and phosphorus dynamics in a flood-pulse system:  
648 Tonle Sap Lake, Cambodia, *J. Hydrol.*, 549, 79–91, <https://doi.org/10.1016/j.jhydrol.2017.03.049>,  
649 2017.

650 Corbett, D.R, Burnett, W., Cable, P., Clark, S.: A multiple approach to the determination of radon fluxes  
651 from sediments. *Journal of Radioanalytical and Nuclear Chemistry*, 236(1–2), 247–253,  
652 <https://doi.org/10.1007/bf02386351>, 1998.

653 Dimova, N. T. and Burnett, W. C.: Evaluation of groundwater discharge into small lakes based on the  
654 temporal distribution of radon-222, *Limnol. Oceanogr.*, 56, 486–494,  
655 <https://doi.org/10.4319/lo.2011.56.2.0486>, 2011.

656 Donohue, I., and Garcia Molinos, J.: Impacts of increased sediment loads on the ecology of lakes.  
657 *Biological reviews*, 84(4), 517-531, <https://doi.org/10.1111/j.1469-185X.2009.00081.x>, 2009.

658 Gao, X., Jia, T., Xu, Q., Wang, F., and Wang, A.: Records of lacustrine sedimentology and  
659 pollen–charcoal assemblages responding to climate change and human activities in Zhongzhouzi  
660 Oxbow Lake, Hubei Province for about 70 years, *Quaternary Sci.*, 36, 1445–1455,  
661 <https://doi.org/10.11928/j.issn.1001-7410.2016.06.10>, 2016.

662 Gonneea, M. E., Morris, P. J., Dulaiova, H., and Charette, M. A.: New perspectives on radium behavior  
663 within a subterranean estuary, *Mar. Chem.*, 109, 250–267,  
664 <https://doi.org/10.1016/j.marchem.2007.12.002>, 2008.

665 Hu, M., Zhou, P., and Chen, C.: Study on coupling of typical elements in surface water and  
666 groundwater in the middle reaches of the Yangtze River, China, *J. Hydrol.*, 623, 130298,  
667 <https://doi.org/10.1016/j.jhydrol.2023.130298>, 2023.

668 Jia, T., Wang, F., and Yuan, S.: Sedimentation and its environmental significance of the Niuyu Lake  
669 along the middle reaches of the Yangtze River: a case study of Tian’e Island and Zhongzhouzi in  
670 the Jingjiang section of the Yangtze River, *Geogr. Res.*, 34, 861–871, 2015. (in Chinese)

671 Jiang, C., Jiang, C., Wang, Q., Liu, H., Li, D., Zhu, Q., and Liu, F.: Seasonal characteristics of  
672 groundwater discharge controlled by precipitation and its environmental effects in a coal mining  
673 subsidence lake, eastern China, *Sci. Total Environ.*, 915, 170067,  
674 <https://doi.org/10.1016/j.scitotenv.2024.170067>, 2024.

675 Jiang, X., Ma, R., Ma, T., and Sun, Z.: Modeling the effects of water diversion projects on surface

676 water and groundwater interactions in the central Yangtze River Basin, *Sci. Total Environ.*, 830,  
677 154606, <https://doi.org/10.1016/j.scitotenv.2022.154606>, 2022.

678 Kazmierczak, J., Postma, D., Muller, S., Jessen, S., Nilsson, B., Czekaj, J., and Engesgaard, P.:  
679 Groundwater-controlled phosphorus release and transport from sandy aquifer into lake, *Limnol.*  
680 *Oceanogr.*, 65, 1447–1463, <https://doi.org/10.1002/lno.11447>, 2020.

681 Kluge, T., Ilmberger, J., von Rohden, C., and Aeschbach-Hertig, W.: Tracing and quantifying  
682 groundwater inflow into lakes using a simple method for radon-222 analysis, *Hydrol. Earth Syst.*  
683 *Sci.*, 11, 1621–1631, <https://doi.org/10.5194/hess-11-1621-2007>, 2007.

684 Lewandowski, J., Rosenberry, D. O., and Meinikmann, K.: Groundwater–lake interfaces, in:  
685 *Ecohydrological Interfaces*, edited by: Krause, S., Hannah, D. M., and Fleckenstein, J. H., Wiley,  
686 Hoboken, NJ, 103–122, <https://doi.org/10.1002/9781119639308.ch6>, 2024.

687 Li, Y., Zhang, Q., Liu, X., and Yao, J.: Water balance and flashiness for a large floodplain system: A  
688 case study of Poyang Lake, China. *Sci. Total Environ.*, 710, 135499, 2020.

689 Luo, X., Kuang, X. X., Jiao, J. J., Liang, S. H., Mao, R., Zhang, X. L., and Li, H. L.: Evaluation of  
690 lacustrine groundwater discharge, hydrologic partitioning, and nutrient budgets in a proglacial  
691 lake in the Qinghai–Tibet Plateau using <sup>222</sup>Rn and stable isotopes, *Hydrol. Earth Syst. Sci.*, 22,  
692 5579–5598, <https://doi.org/10.5194/hess-22-5579-2018>, 2018.

693 MacIntyre, S., Wanninkhof, R., & Chanton, J.P.: Trace gas exchange across the air-water interface in  
694 freshwater and coastal marine environments, in, edited by: Matson, PA and Harriss, RC, *Biogenic*  
695 *trace gases: Measuring emissions from soil and water*, *Methods Ecol. Evol.*, 52–97, 1995.

696 Meinikmann, K., Hupfer, M., and Lewandowski, J.: Phosphorus in groundwater discharge – a potential  
697 source for lake eutrophication, *J. Hydrol.*, 524, 214–226,  
698 <https://doi.org/10.1016/j.jhydrol.2015.02.031>, 2015.

699 Petermann, E., Gibson, J. J., Knöller, K., Pannier, T., Weiß, H., and Schubert, M.: Determination of  
700 groundwater discharge rates and water residence time of groundwater-fed lakes by stable isotopes  
701 of water (<sup>18</sup>O, <sup>2</sup>H) and radon (<sup>222</sup>Rn) mass balances, *Hydrol. Process.*, 32, 805–816,  
702 <https://doi.org/10.1002/hyp.11401>, 2018.

703 Qin, B., Zhou, J., Elser, J. J., Gardner, W. S., Deng, J., and Brookes, J. D.: Water depth underpins the  
704 relative roles and fates of nitrogen and phosphorus in lakes, *Environ. Sci. Technol.*, 54, 3191–3198,  
705 <https://doi.org/10.1021/acs.est.9b05835>, 2020.

706 Redfield, A. C.: The biological control of chemical factors in the environment, *Sci. Prog.*, 11, 150–170,  
707 1960.

708 Rosenberry, D. O., Lewandowski, J., Meinikmann, K., and Nützmann, G.: Groundwater – the  
709 disregarded component in lake water and nutrient budgets. Part 1: effects of groundwater on  
710 hydrology, *Hydrol. Process.*, 29, 2895–2921, <https://doi.org/10.1002/hyp.10403>, 2015.

711 Schmidt, A., Gibson, J. J., Santos, I. R., Schubert, M., Tattrie, K., and Weiss, H.: The contribution of  
712 groundwater discharge to the overall water budget of two typical boreal lakes in Alberta, Canada  
713 estimated from a radon mass balance, *Hydrol. Earth Syst. Sci.*, 14, 79–89,  
714 <https://doi.org/10.5194/hess-14-79-2010>, 2010.

715 Shi, X., Luo, X., Jiao, J. J., and Zuo, J.: Dominance of evaporation on lacustrine groundwater discharge  
716 to regulate lake nutrient state and algal blooms, *Water Res.*, 219, 118620,  
717 <https://doi.org/10.1016/j.watres.2022.118620>, 2022.

718 Stets, E. G., Winter, T. C., Rosenberry, D. O., and Striegl, R. G.: Quantification of surface water and  
719 groundwater flows to open- and closed-basin lakes in a headwaters watershed using a descriptive  
720 oxygen stable isotope model, *Water Resour. Res.*, 46, W03504,  
721 <https://doi.org/10.1029/2009WR007793>, 2010.

722 Sun, X., Du, Y., Wu, J., Xu, J., Tian, H., Han, P., and Wang, Y.: Spatial variability of lacustrine  
723 groundwater discharge at basin scale, *J. Hydrol.*, 629, 134404,  
724 <https://doi.org/10.1016/j.jhydrol.2024.134404>, 2025a.

725 Sun, X., Du, Y., Xu, J., Tian, H., Deng, Y., Gan, Y., and Wang, Y.: Control of groundwater–lake  
726 interaction zone structure on spatial variability of lacustrine groundwater discharge in oxbow lake,  
727 *Water Resour. Res.*, 61, e2024WR039334, <https://doi.org/10.1029/2024WR039334>, 2025b.

728 Tecklenburg, C. and Blume, T.: Identifying, characterizing and predicting spatial patterns of lacustrine  
729 groundwater discharge, *Hydrol. Earth Syst. Sci.*, 21, 5043–5063,  
730 <https://doi.org/10.5194/hess-21-5043-2017>, 2017.

731 Wang, Q., Li, H., Zhang, Y., Wang, X., Zhang, C., Xiao, K., and Qu, W.: Evaluations of submarine  
732 groundwater discharge and associated heavy metal fluxes in Bohai Bay, China, *Sci. Total Environ.*,  
733 695, 133873, <https://doi.org/10.1016/j.scitotenv.2019.133873>, 2019.

734 Webster, I. T., Hancock, G. J., and Murray, A. S.: Modelling the effect of salinity on radium desorption  
735 from sediments, *Geochim. Cosmochim. Acta*, 59, 2469–2476,

736 [https://doi.org/10.1016/0016-7037\(95\)00111-7](https://doi.org/10.1016/0016-7037(95)00111-7), 1995.

737 Xiong, L., Aldahan, A., Qian, R., Yi, P., Chen, X., Li, K., and He, P.: Spatio-temporal patterns and  
738 quantification of lake-groundwater interaction determined in a large water transfer lake, *Hydrol.*  
739 *Process.*, 37, e14867, <https://doi.org/10.1002/hyp.14867>, 2023.

740 Xu, R., Du, Y., Wang, Z., Sun, X., Yang, L., Liu, J., and Gan, Y.: Contrasting lacustrine groundwater  
741 discharge in two small perennial lakes around dried-up Chahannaoer Lake, Northern China, *J.*  
742 *Hydrol. Reg. Stud.*, 58, 102280, <https://doi.org/10.1016/j.ejrh.2025.102280>, 2025.

743 Xu, Y., Wu, Y., Han, J., and Li, P.: The current status of heavy metal in lake sediments from China:  
744 Pollution and ecological risk assessment. *Ecology and evolution*, 7(14), 5454-5466.  
745 <https://doi.org/10.1002/ece3.3124>, 2017.

746 Xue, P., Wen, Z., Zhao, D., Jakada, H., and Liang, X.: Determination of hydraulic conductivity and its  
747 spatial variability in the Jiangnan Plain using a multi-format, multi-method approach, *J. Hydrol.*,  
748 594, 125917, <https://doi.org/10.1016/j.jhydrol.2021.125917>, 2021.

749 Zedler, J. B. and Kercher, S.: Wetland resources: status, trends, ecosystem services, and restorability,  
750 *Annu. Rev. Environ. Resour.*, 30, 39–74,  
751 <https://doi.org/10.1146/annurev.energy.30.050504.144248>, 2005.

752 Zhang, Q., Zhao, Y., Li, Y., and Li, X.: Application of radon-222 to assess groundwater discharge  
753 and associated nutrients input in the karst wetland, China *Environ. Sci.*, 44(6), 3226-3239,  
754 <https://doi.org/10.19674/j.cnki.issn1000-6923.20240301.004>. (in Chinese)

755 Zheng, J., Chen, K., Wu, J., and Wu, J.: Lacustrine groundwater discharge as an important hidden  
756 source of nutrients to a large eutrophic lake: implications for eutrophication management, *Sci.*  
757 *Total Environ.*, 960, 178313, <https://doi.org/10.1016/j.scitotenv.2024.178313>, 2025.